Physicochemistry of the Interaction between Inulin and Alkyltrimethylammonium Bromides in Aqueous Medium and the Formed Coacervates

Abhijit Dan, Soumen Ghosh, and Satya P. Moulik*

Center for Surface Science, Department of Chemistry, Jadavpur University, Kolkata 700032, India

Received: March 24, 2009; Revised Manuscript Received: May 6, 2009

Inulin, a polydisperse reserve polysaccharide, has prospective uses in food, pharmacy, and industry. Its uses and applications often encounter interactions with lipids and amphiphiles. Reports on such interactions are scarcely found in literature. In the present study, we have examined the nature of interactions between inulin and cationic amphiphiles, alkyltrimethylammonium bromides (C_nTAB: $n = 12, 14, 16, 18$), over a fair range of concentrations for both the polymer and the amphiphile. At low concentration, small induced amphiphile aggregates form complexes with inulin; at moderate concentration, the complexed inulin self-aggregates leading to coacervate formation, and at higher concentration, the amphiphile forms free micelles in solution. Tensiometric, conductometric, viscometric, and turbidimetric methods have been employed to study the above phenomena. The isolated coacervates of inulin with C_{18}TAB were examined by scanning electron microscopy (SEM), transmission electron microscopy (TEM), atomic force microscopy (AFM), differential scanning calorimetry (DSC), thermogravimetry (TG), and differential thermal analysis (DTA) to ascertain their morphology, structure, and thermal stability.

Introduction

Polymer−surfactant interaction is a fascinating area of research. Both synthetic and natural polymers and different types of surfactants are used in these studies. The interaction may lead to the formation of easy flowing, viscous, and gel-forming products with prospects for uses in industry, pharmacy, and medicine. The interaction can in many instances form coacervates that themselves constitute an interesting field for study. The coacervates constitute a phase of special identity and can be used for solubilization and encapsulation of lipophilic drugs and their convenient delivery as well as for the synthesis of nanoparticles therein. In drug delivery,[1−3] cosmetic formulation (with special reference to body and skin care products),[4−6] nanomaterial preparation,[7−9] pharmaceutical[10] and industrial fields,[11−13] etc., polymer−surfactant (or lipid) interaction is involved in one way or another. Water-soluble synthetic and modified polymers, viz., polyethylene oxide,[14−17] polyethyleneglycols,[18,19] polyvinylpyrrolidone (PVP),[20−26] carboxymethyl cellulose,[27−29] the *N*,*N*-dimethyl-*N*-methyl derivative of hydroxyethylcellulose (JR 400),[30,31] the *N*,*N*-dimethyl-*N*-dodecyl derivative of hydroxyethylcellulose (LM 200),[30,31] etc., carbohydrate polymers, viz., starch,[32−34] amylose,[35−37] amylopectin,[38−40] etc., and proteins, viz., bovine serum albumin,[41−44] lysozyme,[43−45] gelatin,[44−46] hemoglobin,[44,47] pepsin,[48] papain,[49−51] egg albumin,[43] etc., have been amply used for their interaction with different amphiphiles. The strength of binding, changes in the configuration of the polymers upon interaction, types of products formed, their evolved physicochemical properties, etc. have been investigated and assessed. In these endeavors, block copolymers[52] and graft copolymers[53] have also been employed but their uses have been much less in comparison with other polymers.

In a recent study,[54] graft copolymers oligo(9,9-dihexyl)fluorence-*graft*-poly(ethylene oxide) (OHF-*g*-PEO) have been reported to exist in an aqueous medium mostly in the form of aggregated globules along with a minor fraction of monomers also of globular geometry. We have recently observed[55] that the carbohydrate polymer inulin also forms aggregated globules in an aqueous medium at a low concentration. This biopolymer has industrial[56] and medicinal[57] uses. It is antidiabetic and is a prospective carbohydrate supplement in food.[58] In the course of our studies on natural polymers and their interaction with surfactants, we have considered the interaction of inulin with the cationic surfactants alkyltrimethylammonium bromides (C_nTAB) of varied alkyl chain lengths (C_{12} to C_{18}). The surfactants interact with the globular inulin aggregates, with their monomers, and with their assemblies to form complexes and coacervates that disintegrate into smaller species in the excess presence of the surfactants following a number of sequential steps. The details of the interaction process have been presented along with the types of product formed with respect to their shapes, sizes, and thermal stability.

Experimental Section

Materials. The inulin (a polysaccharide extracted from chicory) used was a 99% pure product of Sigma (St. Louis, MO). AR-grade cetyltrimethylammonium bromide (CTAB, purity >99%) of Aldrich (St. Louis, MO) and AR-grade dodecyltrimethylammonium bromide (DTAB, purity >99%), tetradecyltrimethylammonium bromide (TTAB, purity >98%), and octadecyltrimethylammonium bromide (OTAB, purity >97%) of Fluka (Buchs SG, Switzerland) were used. The materials were used as received. All solutions were prepared in doubly distilled water with a specific conductance of 2−4 μS cm^{-1} at 303 K. The concentration of inulin used has been expressed in percent (w/v) throughout the text.

Methods. ***Tensiometry.*** Tensiometric measurements were taken with a calibrated du Noüy tensiometer (Krüss, Germany) by the platinum ring detachment technique previously

* To whom correspondence should be addressed. E-mail: spmcss@yahoo.com. Fax: +91-33-2414-6266.

10.1021/jp902641d CCC: $40.75
Published on Web 05/28/2009

described.[26,29,30] A water or inulin solution was placed in a double-walled thermostated container to which the surfactant solution was added stepwise as required using a Hamilton mycrosyringe. The measurements were taken following a 20 min time interval for equilibration after through mixing. The accuracy of the measured γ was ± 0.1 mN m^{-1}.

Conductometry. The conductivity measurements were performed with a Jenway (Essex, U.K.) conductometer in a conductivity cell of unit cell constant. The same procedure, as in tensiometry, of the addition of a surfactant solution to 10 mL of either a water or inulin solution of desired strength was followed. The accuracy of measurements was within $\pm 0.5\%$.

Viscometry. The viscosity measurements were taken in a calibrated Ubbelohde viscometer (placed in a water bath) with a clearance time of 186.1 s for 13 mL of water in a temperature controlled water bath with an accuracy of ± 0.1 °C. An inulin solution of the desired strength was placed in the viscometer, and a concentrated surfactant solution was progressively added in stages with a Hamilton microsyringe; the flow times for the additions were measured after thorough mixing and thermal equilibration. The accuracy of viscosity measurements was within $\pm 0.5\%$.

Turbidimetry. The turbidimetric experiments were performed in a Shimadzu 1601 (Tokyo, Japan) spectrophotometer operating in dual beam mode using a matched pair of quartz cuvettes with a path length of 1 cm under a thermostated condition (303 $\pm$ 0.1 K). The measurements were taken in transmittance (%T) mode. In an actual experiment, the concentrated surfactant solution was progressively added with a microsyringe into the sample cell containing 2.5 mL of an inulin solution of desired strength, and the solution was mixed using a magnetic stirrer. It was allowed to sit for 5 min before taking a measurement. The turbidity index (100 $-$ %T at $\lambda_{max} = 325$ nm of inulin solution) was plotted against [C_nTAB]. The measured values were corrected with a blank corresponding to the dilution of inulin by the addition of water.

Transmission Electron Microscopy (TEM). TEM images of surfactant-interacted inulin were obtained using a JEOL JEM 2010 (Tokyo, Japan) high resolution transmission electron microscope (HRTEM) operating at 200 kV. Two drops of a solution were placed onto a carbon-coated copper grid, and it was then dried prior to the measurement being taken.

Scanning Electron Miscroscopy (SEM). SEM measurements were taken with a JEOL JEM 6700F (Tokyo, Japan) field-emission scanning electron microscope (FESEM). A drop of the inulin$-C_n$TAB interacted sample was spin-coated on a stab followed by being coated with gold.

Atomic Force Microscopy (AFM). The topological images of the samples on the glass surface were performed on a Nanosurf easyScan 2 (Rüschlikon, Switzerland) AFM in contact mode with a constant force of 20 nN. A drop of the inulin$-C_n$TAB sample was placed onto the glass surface and was imaged after being annealed.

Thermogravimetry Analysis (TGA) and Differential Thermal Analysis (DTA) (TGA$-$DTA). TGA and DTA of the sample of the isolated inulin$-C_n$TAB complex were performed with a Perkin Elmer Pyris Diamond TG/DTA thermal analyzer (Waltham, MA). The sample was heated to 500 °C at a rate of 20 °C/min under flowing N_2 gas.

Differential Scanning Calorimetry (DSC). A Perkin Elmer DSC-7 (Waltham, MA) fitted with an intracooler-1 was used under an N_2 atmosphere. The instrument was calibrated with indium. About a 3 mg sample of the inulin$-C_n$TAB complex was placed in an aluminum pan, and it was sealed. After equilibration for 10 min, the sample was heated at a rate of 10 °C/min from ~30 to ~200 °C. It was then cooled at a rate of 5 °C/min and followed by heating again with the same rate as the first time. The thermograms were recorded, and the peak temperatures and enthalpies were obtained from the system computer.

TABLE 1: Critical Micellar Concentration (cmc) and Related Thermodynamic Parameters for Pure C_nTAB in Aqueous Solution at 303 K[a,b]

	cmc							
	ST	cond	γ_{cmc}	Γ_{max} ($\times 10^6$)	A_{min}	β	ΔG^0_m	ΔG^0_{ad}
DTAB	15.3	15.1	39.0	1.51	1.11	0.71	−35.4	−57.3
TTAB	3.72	3.85	37.2	1.37	1.21	0.75	−42.3	−67.6
CTAB	0.98	0.97	35.0	1.23	1.35	0.77	−48.9	−78.9
OTAB	0.32	0.28	31.0	1.12	1.48	0.67	−50.6	−87.1

[a] cmc, γ_{cmc}, Γ_{max}, A_{min}, ΔG^0_m, and ΔG^0_{ad} are expressed in mmol dL^{-1}, mN m^{-1}, mol m^{-2}, nm^2 molecule^{-1}, kJ mol^{-1}, and kJ mol^{-1}, respectively. [b] Standard deviations of the parameters: cmc (ST) = $\pm 5\%$; cmc (cond) = $\pm 7\%$; $\gamma_{cmc} = \pm 5\%$; $\Gamma_{max} = \pm 8\%$; $A_{min} = \pm 6\%$; $\Delta G^0_m = \pm 3\%$; $\Delta G^0_{ad} = \pm 7\%$.

Results and Discussion

A. C_nTAB in Aqueous Solution. In relation to one describing the behaviors of C_nTABs in an inulin environment, their interfacial and bulk behaviors in an aqueous solution without the polymer deserve documentation. Although results are scattered in the literature,[59−61] a consolidated account herein realized is presented. These are critical micellar concentration (cmc), maximum surface excess (Γ_{max}), minimum headgroup area (A_{min}), standard Gibbs free energy of micellization (ΔG^0_m) and adsorption (ΔG^0_{ad}), counterion binding (β), and surface tension at cmc (γ_{cmc}). The following relations were used for the calculations.[59−62] Graphical presentations are not shown to save space. Thus,

$$\Gamma_{max} = -\frac{1}{2.303nRT}\lim_{C\to cmc}\frac{d\gamma}{d(\log C)} \quad (1)$$

$$A_{min} = \frac{10^{18}}{N\Gamma_{max}} \quad (2)$$

$$\beta = 1 - S_2/S_1 \quad (3)$$

$$\Delta G^0_m = (1+\beta)RT\ln X_{cmc} \quad (4)$$

$$\Delta G^0_{ad} = \Delta G^0_m - \frac{\Pi_{cmc}}{\Gamma_{max}} \quad (5)$$

where the new terms γ = surface tension, C = surfactant concentration in mole fraction, N = Avogadro's number, S_2/S_1 = ratio of the linear post- and pre-cmc plots of conductance vs salt concentration, Π_{cmc} = surface pressure at cmc (the difference between $\gamma_{water} - \gamma_{cmc}$), and T = absolute temperature.

The determined parameter values are presented in Table 1. The β values meant 67−75% binding of Br^- ions with the micelles. The γ_{cmc} also decreased with increasing chain length, i.e., hydrophobicity. The Γ_{max} and A_{min} were complementary to each other; their products were comparable with an average of 1.66×10^{-6} mol nm^{-1}. Both micellization and interfacial

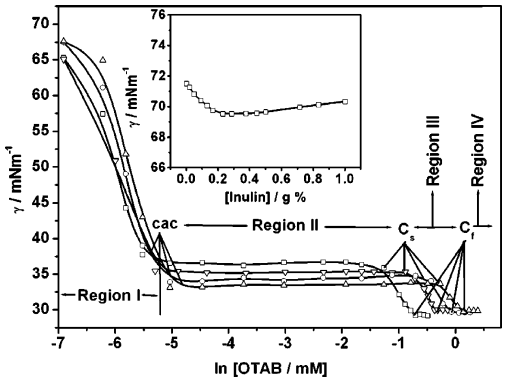

Figure 1. Tensiometric profiles of the inulin−OTAB interaction at 303 K with varied inulin concentration in aqueous medium: □, 0.25% (w/v); ▽, 0.5% (w/v), ○, 0.75% (w/v); Δ, 1.0% (w/v). Inset: surface tension (γ) of inulin at 303 K as a function of polymer concentration.

processes were spontaneous which increased with increasing hydrophobicity. The efficiency ratio of the two processes ($\Delta G^0_{ad}/\Delta G^0_m$) was on the average 1.64.

B. C_nTAB in Aqueous Inulin Environment. ***Behavior of OTAB.*** For polymer−amphiphile interaction, tensiometry has a distinction. It can reveal the nature of the interaction of the amphiphile with the polymer both at the interface and in the bulk. The following presentation is with reference to the results of the inulin−OTAB system.

The inulin was mildly surface active. A 0.2% (w/v) inulin solution reduces γ of water by 2 mN m^{-1} (Figure 1, inset). It, thus, essentially remains in the bulk.

The results of the interaction of OTAB with inulin concentrations from 0.25 to 1.0% (w/v) are illustrated in the main plot of Figure 1, which has four distinct regions. In region I, with an initial small addition of OTAB, only a minor amount of OTA^+ ions interacted with the self-aggregated inulin.[55] With progressive surfactant addition, the interracially adsorbed OTAB continued to decrease γ up to a certain concentration at which it started to form small assemblies which is called the critical aggregation concentration (cac). In the post-cac stage (region II), the aggregates continued to bind with the polymer sites that restricted the transfer of OTA^+ ions to the interface to maintain a constant γ for a fairly large [OTAB] in the range of $\sim 10^{-5}$ to 10^{-1} M. In this regime, the configuration of the polymer species changed; the amphiphile assemblies remained adhered to the biopolymer with partial depletion of Br^- ions from their electrical double layer. Such a phenomenon of polymer−surfactant systems in an aqueous medium has been demonstrated in the literature.[14−26] The phenomenon occurs at surfactant concentrations ≪ cmc as herein observed. The cac values were found to mildly depend on inulin concentration as reported for other polymers.[26,29,63−65] Unlike OTAB for many other polymer−surfactant systems, ups and downs in γ in the post-cac region have been reported.[26,46,48] There, the polymers themselves are fairly surface active. Upon interaction with the ionic micellar aggregates at concentrations ≥ cac, the interacted products get released from the interface and sink in the bulk. Their depletion enhances γ, which rises to a maximum when the process is complete. Thereafter, the incoming surfactant molecules get adsorbed at the interface to cause a reduction in γ. The inulin was weakly surface active and, hence, interaction of small micelles of OTAB, with it in the interfacial region, mildly affected γ in the post-cac stage until free OTAB molecules started accumulating at the interface at C_S and ended at C_f where free micelles of OTAB started to form in solution. The polymer−surfactant complexes in solution can self-assemble to form a turbid coacervate phase that further interacts with large surfactant micelles at the increased surfactant concentration in the post-C_f stage to get converted into a transparent solution. In the past, Goddard[66,67] reported tensiometric features of several water-soluble polymer−surfactant systems. Guillot et al.[68] also reported a fairly flat region beyond cac as in Figure 1. The coacervates of the inulin−OTAB complex were colloidal dispersions, having the tendency to separate out from the solution but, to start with, remained visually undetectable. With increased inulin concentration, the number of available binding sites increased leading to enlarged cac−C_S region. The binding of the induced small micelles to the polymer loosened the globular inulin aggregates in solution that efficiently reassociated to produce visible coacervates at the point of C^* in the turbidity measurements (discussed later). The micelle-bound stretched polymer molecules became partially surface active, by virtue of their exposed hydrophobic segments, to cause a reduction in γ with increasing inulin concentration to end up lowering the height of the cac−C_S region (Figure 1). At C_S, the binding of the induced small micelles to the polymer was complete. Thereafter, in region III, the surfactant monomers accumulated at the air/water interface and reduced γ, which was complete at C_f (extended cmc). Beyond that point, OTAB hardly affected γ, and free micelles were formed in solution (region IV). Both C_S and C_f values for the inulin−OTAB system increased with increasing inulin concentration as expected from the mass balance consideration (Table 2). The γ_{cmc} of OTAB for different inulin concentrations was more or less equal ($\sim$30 mN m^{-1}), indicating a similar type of micelle in solution with comparable interfacial composition. The transformation of the coacervates to a turbid colloidal dispersion was also observed in the gelatin−CTAB system.[46] The cac, C_S, and C_f values determined by tensiometry are presented in Table 2 along with the results by other methods.

Conductometry is a potential method for probing the bulk property of interaction between a neutral polymer and an ionic surfactant. The conductometry profile of OTAB with inulin has shown three distinct inflections (Figure 2). Of the three break points, two fairly agreed with the C_S and C_f of tensiometry. The first break at C^* also appeared in both turbidimetry and viscometry (see next sections). No break in the plot at or close to cac was observed in conductometry, similar to the case with the gelatin−C_nTAB system.[46] Initially, conductance of the OTAB solution increased linearly with concentration. After the first break at C^*, the conductance linearly increased with a higher slope. At C^*, visible appearance of turbidity started in the system which meant the initiation of unfolding and an efficient aggregation of the complex. The increased slope in the post-C^* region was due to the contribution of the surface conductance observed in colloidal dispersions;[69,70] the coacervate-containing system was essentially a colloidal solution. The value of C^* was only marginally changed with an increase in inulin concentration (Table 2). Between C_S and C_f, the conductance course appeared with a lower slope. At higher [OTAB] > C_S (0.45 mM), the surface conductance became nominal in comparison with ion conductance; there, the colloidal coacervate obstructed the ion transport[71,72] to produce a line with a lower slope up to C_f. Beyond C_f, free micelle formation commenced in the system with a fair degree of counterion binding to yield a straight line in the conductance−concentration plot with a further reduced slope.[26,29,46,49]

The solution viscosity was also responsive to the bulk complexation process because of changes in the configuration

TABLE 2: Critical C_nTAB Concentrations[a] Associated with the Interaction Processes Obtained from Different Methods at 303 K[b]

	tensiometry[c]				
[inunin]/% (w/v)	cac	C_S	C_f	conductometry C_f	turbidimetry C_T
			Inulin−DTAB Interaction		
0.25	1.00	5.42	15.5		8.15
0.5	1.02	4.83	15.2	15.37	7.95
0.75	1.08	4.83	15.2		8.05
1	1.11	5.42	15.5	15.81	7.85
			Inulin−TTAB Interaction		
0.5	0.07	0.69	3.8	4.31	1.38
1	0.10	0.78	4.2	4.74	1.67
			Inulin−CTAB Interaction		
0.5	0.017	0.42	1.44	1.38	0.48
1	0.021	0.51	1.68	1.68	0.82
			Inulin−OTAB Interaction		

	tensiometry[c]			conductometry			turbidimetry		viscometry		
[inunin]/% (w/v)	cac	C_S	C_f	C^*	C_S	C_f	C^*	C_T	C^*	C_S	C_f
0.25	0.004	0.28	0.49	0.17	0.31	0.51	0.16	0.32	0.18	0.28	0.51
0.5	0.005	0.49	0.65	0.18	0.49	0.66	0.19	0.47	0.18	0.44	0.63
0.75	0.006	0.65	0.89	0.21	0.69	0.88	0.20	0.64			
1	0.008	0.90	1.15	0.23	0.90	1.10	0.21	0.83			

[a] The concentration terms have been designated as follows: cac, critical aggregation concentration; C_S, polymer saturation concentration; C_f, critical concentration of free micelle formation; C_T, critical concentration of maximum turbidity; C^*, critical concentration of polymer unfolding. [b] All the parameters are presented in mmol dL^{-1}. Their standard deviations are in the range of ±5−10%. [c] The interaction strengths ($[C_f - cac]/cac$) were 13.9, 53.3, 83.7, and 129.0 for the interaction of DTAB, TTAB, CTAB, and OTAB, respectively, with 0.5% (w/v) inulin.

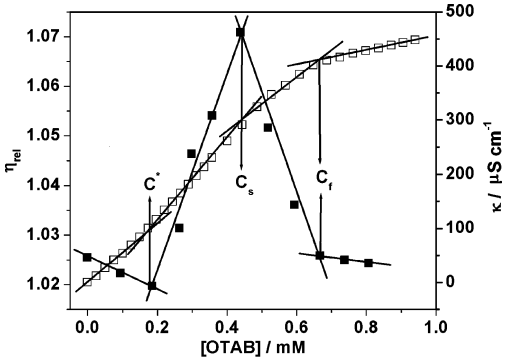

Figure 2. Conductometric and viscometric representrations for a 0.5% (w/v) inulin−OTAB system at 303 K: □, conductometry; ■, viscometry.

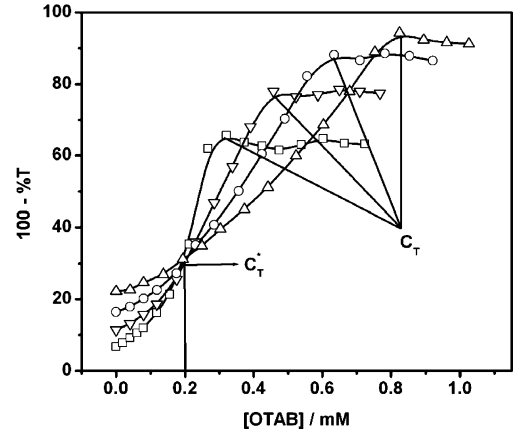

Figure 3. Turbidimetric plots for the interaction between inulin and OTAB at 303 K with varied inulin concentration in an aqueous medium: □, 0.25% (w/v); ▽, 0.5% (w/v), ○, 0.75% (w/v); Δ, 1.0% (w/v).

of the complex. The relative viscosity of a 0.5% (w/v) inulin solution with progressive addition of OTAB plotted against [OTAB] is also depicted in Figure 2. The profiles at all other inulin concentrations were the same. Four regions with three distinct inflections were observed in the profile. In the absence of OTAB, the globular inulin (I) aggregates existed in solution along with a minor amount of monomers.[55] The small addition of OTAB helped to contract the globules further up to C^*, the point of unfolding of the complex. Beyond C^*, the polyelectrolyte-like (I−small micelle) complex progressively unfolded and aggregated to impart increased viscosity (and turbidity mentioned earlier). The viscosity maximized at C_S (the point of maximum turbidity). In the post-C_S region, the viscosity decreased by way of disintegration of the heterogeneous-aggregated complex into species of smaller dimensions (supported by TEM results in section E and Figure 6). The viscosity reached a low value at C_f and only slightly declined from this point of free micelle formation. Such a phenomenon was also observed for the polyacrylamide methyl propane sulfonate (PAMPS).[73] The C^*, C_S, and C_f values for different inulin concentrations are presented in Table 2. The cac points that appeared in tensiometry were not found in viscometry as well as in the conductivity and turbidity profiles subsequently discussed.

In the inulin−OTAB solution, turbidity arose due to coacervation. The turbidimetric profiles in the bulk solution are depicted in Figure 3. The turbidimetry followed a nearly sigmoidal course at all inulin concentrations. The courses produced a crossing point (C_T^*) that roughly corresponded to C^* (Figure 2). The beginning of the maximum in the plot (C_T) corresponded with C_S (Figure 2) where turbidity was clearly visible. The C_T increased with increasing inulin concentration, whereas C_T^* only marginally increased with increasing polymer concentration (Table 2). The turbidity slightly declined in the post-C_T stage. There were reports[29,74,75] of a large depletion of visible turbidity owing to the formation of free micelles solubilizing the coacervates. In our study, the coacervates were only partially solubilized and the measured turbidity was not

SCHEME 1: Illustration of the Interaction of OTAB with Inulin at the Interface and in the Bulk[a]

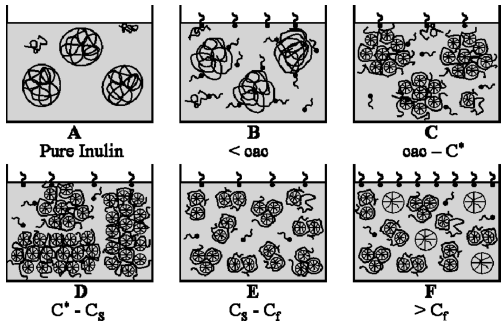

[a] (A) Inulin in water at the start of region I. (B) Inulin with [OTAB] approximately at cac (near completion of region I). (C) Assemblies of necklace−bead complexes in the cac−C^* domain of region II. (D) Further aggregation of complexes in the C^*-C_S domain of region II. (E) Disintegration of large aggregates into lower species in the C_S-C_f domain of region III. (F) Normal micelles coexist with smaller complex aggregates beyond C_f in region IV.

largely reduced in the post-C_T stage. The population of the aggregates in solution was sufficient to register reduced transmission of light. Separation of a minor amount of the inulin−OTAB complex from the solution after standing for a long time was observed.

The above-described events in the regions I−IV with reference to Figure 1 are pictorially presented in Scheme 1.

Behavior of Other C_nTABs. The chain length of the surfactants in a homogeneous series has influenced the effect on the polymer−surfactant interaction. In some respects, the patterns for C_{12}-, C_{14}- and C_{16}TAB were different from those for OTAB; the regions, cac−C_S, in the tensiometry study were slightly wavy in nature. The results supported formation of cac, C_S, and C_f. The effect of inulin concentration on cac, C_S, and C_f was milder than OTAB, but the magnitudes of the parameters depended on the C_nTAB chain length with the order DTAB < TTAB < CTAB < OTAB. The C_f of DTAB was only slightly different from its normal cmc. The γ_{C_f} (surface tension at C_f) values followed the order DTAB > TTAB > CTAB > OTAB. According to Hansson and Almgren,[76] the difference between cac and extended cmc (C_f) is a measure of the strength of interaction between a polymer and a surfactant. The ratio of (C_f − cac)/cac was herein considered as an estimate of the interaction strength of C_nTAB with inulin. The ratio linearly increased with chain length; the values were 13.9, 53.3, 83.7, and 129 for DTAB, TTAB, CTAB, and OTAB, respectively. The hydrophobicity favorably controlled the interaction process.

The inulin−C_nTAB interaction for the C_{12}-, C_{14}-, and C_{16}-homologues in the bulk was also conductometrically studied under identical conditions. The conductometric results on a 0.5% (w/v) inulin interaction with DTAB, TTAB, and CTAB have evidenced a very weak effect (cf. inset Figure 4 for TTAB). OTAB has shown visible interaction (Table 2), with distinct inflections at C^*, C_S, and C_f (cf. Figure 2). The homologues lower than OTAB produced only a single break in the plots with and without inulin. There was no change in the electrochemical state in the solution environment up to the stage of free micelle formation to affect the electrical transport properties of the inulin solution containing the lower homologues. Thus, either the extent of interaction of the lower C_nTABs with inulin was too small to register intermediate changes or the structural and organizational differences of the complexes of inulin were more minor than OTAB. The extended cmc was, thus, detected by the method.

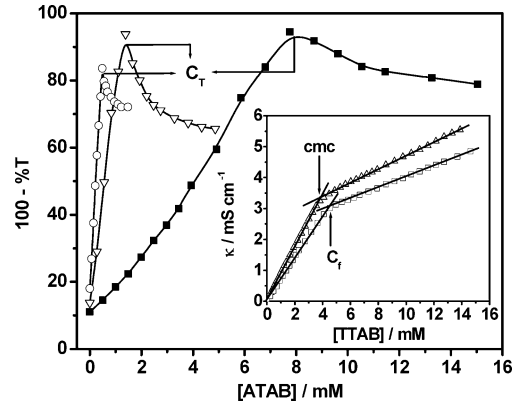

Figure 4. Turbidimetric profiles for the ATAB interaction with 0.5% (w/v) inulin at 303 K with varied chain length of the surfactant: ○, CTAB; ▽, TTAB; ■, DTAB. Inset: conductometric plots for TTAB without and with 0.5% (w/v) inulin at 303 K.

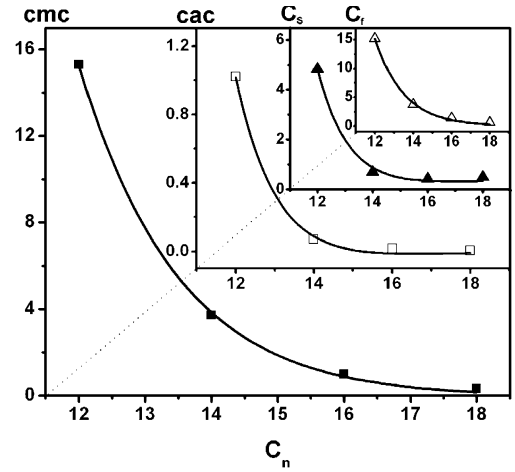

Figure 5. Dependences of cmc, cac, C_S, and C_f of C_nTABs in 0.5% (w/v) inulin with carbon number (C_n) of their alkyl chain at 303 K.

The C_T values determined by turbidimetry of the lower C_nTABs were more different from the C_S values found by tensiometry (Table 2). The C_T for CTAB and OTAB determined by tubidimetry for 0.5% (w/v) inulin compared reasonably well with the C_S determined by tensiometry. This corroboration failed for 1% (w/v) inulin with CTAB. The C_T values for the lower homologues DTAB and TTAB were intermediate between C_S and C_f (cf. Figure 4 and Table 2). For the lower homologues, the turbidity was found to decrease appreciably beyond C_T. The coacervates easily disintegrated and solubilized in higher [C_nTABs]. The phenomenon became prominent with decreasing amphiphile chain length.

The dependences of cac, C_S, and C_f on the carbon number of C_nTABs were all found to be exponential in nature (Figure 5). The decline of these parameters from C_{12}TAB to C_{14}TAB was rapid; thereafter, the fall was mild and marginal.

C. Comprehensive Representation of the Involved Interaction Processes. The processes that arose by the interaction of C_nTAB with inulin in solution at the interface and in the bulk are summarized below.

The following discussion is with reference to the $\gamma-\ln$ [S] pattern of Figure 1. To start with, the addition of a very small amount of surfactant in the system (aqueous solution of inulin) forms a highly dispersed adsorbed amphiphile monolayer at the air/liquid interface (I^{al}) following the equilibrium (i), i.e., PA_1,

$$I^{al} + S \leftrightarrow I^{al}S(1) \qquad \text{Process } PA_1 \qquad \text{(i)}$$

where S represents surfactant to form the surface complex $I^{al}S(1)$. The surface tension γ starts to decline.

Addition of more S sets the equilibrium (ii),

$$I^{i}_{n} + n_1 S \leftrightarrow I^{i}_{n}S_{n_1} \qquad \text{Process PB} \qquad \text{(ii)}$$

where I^{i}_{n} is the inulin at the interface and n_1 is the number of S molecules individually attached to inulin at different centers forming the complex $I^{i}_{n}S_{n_1}$ by the process PB. Both PA_1 and PB continue to decrease γ.

In the bulk, the following equilibrium (process PC) arises by the interaction of bulk inulin, I^{b}_{n}, with n_2 number of S as in PB to form the complex $I^{b}_{n}S_{n_2}$.

$$I^{b}_{n} + n_2 S \leftrightarrow I^{b}_{n}S_{n_2} \qquad \text{Process PC} \qquad \text{(iii)}$$

All the above processes occur in the pre-cac region or region I indicated in Figure 1.

The addition of more amphiphiles at [S] > cac in region II generates small induced micelles that form a kind of "necklace−bead-type" complex[77−79] with the loosely unfolded biopolymer assembly in the form of I*n*b$S n_2$−S(agg)*m* in the bulk where *m* number of amphiphiles produces an induced small micelle of S. The following equilibrium (process in bulk or PD_b) then arises.

$$I^{b}_{n}S_{n_2} + mS(agg)_m \leftrightarrow I^{b}_{n}S_{n_2} - S(agg)_m \qquad \text{Process } PD_b \qquad \text{(iv)}$$

A similar process also arises with $I^{i}_{n}S_{n_1}$ at the interface to form $I^{i}_{n}S_{n_1}$−S(agg)$_m$ designated as process PD_i. Thus,

$$I^{i}_{n}S_{n_1} + mS(agg)_m \leftrightarrow I^{i}_{n}S_{n_1} - S(agg)_m \qquad \text{Process } PD_i$$

The formation of the induced micelles at the cac provides a break in the γ−ln [S] profile, since the surface adsorption process of the amphiphile becomes nonoperative.

With the addition of the amphiphile in solution, the polymer segments get saturated with small aggregates by PD_b and PD_i up to the state of C_S. The ionic micelle laden complexed inulin at the interface may leave the interface and become $I^{b}_{n}S_{n_2}$−S(agg)$_m$. The interface becomes desorped and is expected to cause an increase in γ. For poorly surface active polymers like inulin, this phenomenon is only marginal, and γ remains practically unaffected in region II (cf. Figure 1).

During this stage, the products of PD undergo self-association to form coacervate (process PE) that may become visible (practically for long chain amphiphiles) in the form of turbidity. Thus,

$$y[I^{b}_{n}S_{n_2} - S(agg)_m] \leftrightarrow [I^{b}_{n}S_{n_2} - S(agg)_m]_y \qquad \text{Process PE} \qquad \text{(v)}$$

In region III, monomers of S start accumulating at the interface to manifest the second adsorption process PA_2 as represented in (vi).

$$I^{al} + S \leftrightarrow I^{al}S(2) \qquad \text{Process } PA_2 \qquad \text{(vi)}$$

The adsorption of the amphiphile reduces γ. As the surface gets saturated, the formation of larger micelles in solution starts at C_f and continues to region IV by the process PF.

$$zS^{+} + xBr^{-} \leftrightarrow S_z(Br)_x^{+(z-x)} \qquad \text{Process PF} \qquad \text{(vii)}$$

where $S_z(Br)_x^{+(z-x)}$ is the micelle with condensed counterions in the Stern layer providing the overall micellar charge $+(z-x)$. The break in the γ−ln [S] profile at the beginning of region IV of C_f is the extended cmc of S, i.e., cmc_e.

D. Interfacial Adsorption and Energy Parameters in the Post-Complexation Stage IV. The Gibbs surface excess ($\Gamma^{C_f}_{max}$) for the free micelle formation of C_nTAB between C_S and C_f in the inulin solution was calculated using eq 1 with the consideration of limiting the concentration to C_f. In this region, amphiphile adsorption at the interface was essentially the process that led to free micelle formation in solution. The area of exclusion per C_nTAB headgroup at the air/water interface ($A^{C_f}_{min}$) was calculated by eq 2. The $\Gamma^{C_f}_{max}$ and $A^{C_f}_{min}$ values for the systems are presented in Table 3. $\Gamma^{C_f}_{max}$ of C_nTAB at C_f increased with an increase in surfactant chain length; the trend was opposite

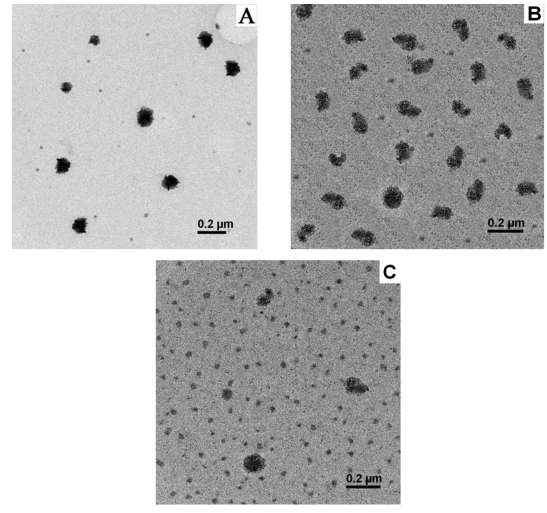

Figure 6. TEM images demonstrating the morphology change of inulin by interaction with OTAB: (A) 0.5% (w/v) pure inulin; (B) with [OTAB] < C_T; (C) with [OTAB] > C_T.

TABLE 3: Interfacial Parameters ($\Gamma^{C_f}_{max}$ and $A^{C_f}_{min}$) and Free Energies of Micellization ($\Delta G^0_{C_f}$) and Adsorption ($\Delta G^0_{ad(I)}$) of the Studied Systems at 303 K[a,b]

inulin−C_nTAB	γ_{C_f}	$\Gamma^{C_f}_{max}$ ($\times 10^6$)	$A^{C_f}_{min}$	$\Delta G^0_{C_f}$	$\Delta G^0_{ad(I)}$
0.5% (w/v) Inulin−C_nTAB					
DTAB	38.4	1.14	1.46	−65.4	−95.0
TTAB	36.4	1.25	1.32	−72.2	−101
CTAB	34.7	1.71	0.97	−132	−154
OTAB	30.0	2.64	0.63	−49.6	−65.5
Variable % (w/v) Inulin−OTAB					
0.25%	29.2	2.78	0.59	−49.0	−64.4
0.5%	30.0	2.64	0.63	−49.6	−65.5
0.75%	29.7	2.37	0.70	−50.7	−68.5
1.0%	29.7	1.87	0.89	−51.2	−73.8

[a] γ_{C_f}, $\Gamma^{C_f}_{max}$, $A^{C_f}_{min}$, $\Delta G^0_{C_f}$, and $\Delta G^0_{ad(I)}$ are expressed in mN m^{-1}, mol m^{-2}, nm^2 molecule^{-1}, kJ mol^{-1}, and kJ mol^{-1}, respectively. [b] Standard deviations of the parameters: $\gamma_{C_f} = \pm 5\%$; $\Gamma^{C_f}_{max} = \pm 8\%$; $A^{C_f}_{min} = \pm 6\%$; $\Delta G^0_{C_f} = \pm 4\%$; $\Delta G^0_{ad(I)} = \pm 7\%$.

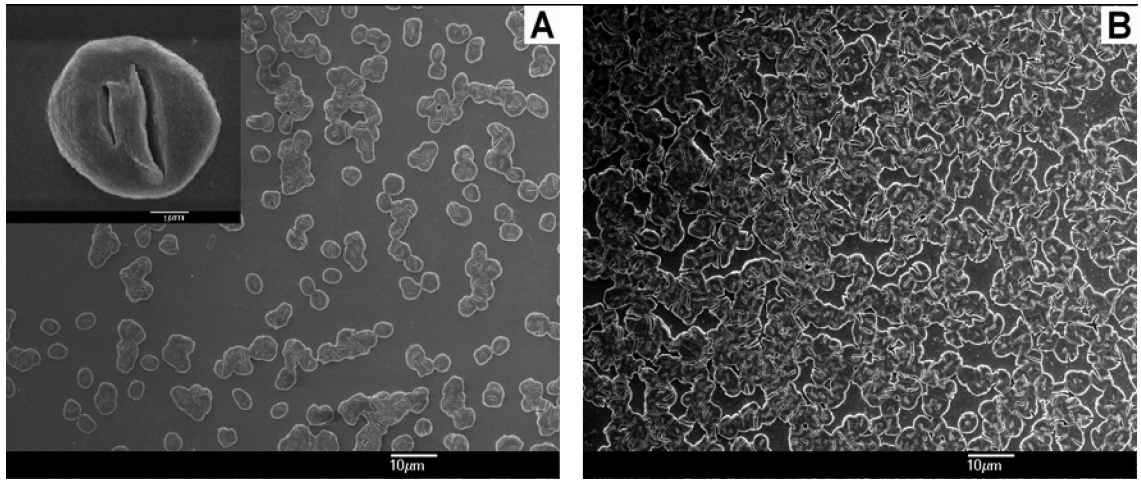

Figure 7. FESEM morphographs demonstrating the morphology change of inulin by the interaction with OTAB: (A) 0.5% (w/v) pure inulin; (B) with [OTAB] > C_T.

to that observed without inulin. Likewise, a decreased trend was also observed for $A_{min}^{C_f}$ without and with inulin. In the aqueous medium, the tilt in the molecules in the adsorbed state normally produces greater A_{min} with an increase in chain length of the homologues. In solution with inulin−C_nTAB complex and its coacervate, the nature of accommodation at the interface became reversed. The $\Gamma_{max}^{C_f}$ quantities were expectedly inversely related with the $A_{min}^{C_f}$ values as found in Table 3. The decline in $\Gamma_{max}^{C_f}$ for OTAB with increasing inulin concentration suggested physicochemical restriction toward the interfacial occupancy of the amphiphile.

The standard Gibbs free energy changes for the process at C_f were calculated from eq 4 using β of C_nTAB in the aqueous solution presented in Table 1. The average values of X_{C_f} (conductometry and tensiometry) were used in the calculation. The $\Delta G_{C_f}^0$ and $\Delta G_{ad(I)}^0$ (calculated from eq 5) for different systems are also presented in Table 3. The spontaneity of the micellization process increased with increasing hydrophobicity of the C_nTAB. The $\Delta G_{ad}^0 > \Delta G_m^0$ in the aqueous solution, so also, the $\Delta G_{ad(I)}^0 > \Delta G_{C_f}^0$ in the inulin environment; their ratios $\Delta G_{ad}^0/\Delta G_m^0$ and $\Delta G_{ad(I)}^0/\Delta G_{C_f}^0$ on the average were 1.52 and 1.35, respectively. They were the respective spontaneity ratios of the adsorption process over micellization without and with inulin in the system. The γ_{cmc} (Table 1) and γ_{C_f} (Table 3) values have shown only minor differences; the formed interfaces were comparable.

E. Morphology of Inulin−OTAB Complex. The morphology of the inulin−OTAB complex was studied by the TEM, SEM, and AFM techniques. The results are presented and discussed below.

TEM. The TEM image of inulin dried from its aqueous solution (Figure 6A) has evidenced fairly uniform globular particles of two grossly sized distributions (monomers and aggregates) in an aqueous medium with average diameters of 22 and 135 nm, respectively.[55] In the presence of [OTAB] below and above the maximum turbidity, C_T (or C_S) morphological changes were observed (Figure 6B,C). Coacervates of larger nonuniform dimensions (Figure 6B) with size distribution in the range of 130−180 nm with comparatively minor tiny globules of monomers were formed at [OTAB] < C_T. At [OTAB] > C_T, the large coacervates disintegrated into smaller aggregates of varied shapes with an average particle size of 30 nm with a tiny fraction of large globules (Figure 6C). The results agreed with the viscosity fall beyond C_S (cf. Figure 2). TEM morphographs of the disintegrated polymer−surfactant complexes have also been reported in recent literature.[80,81] The disintegrated entities were also globular aggregates.

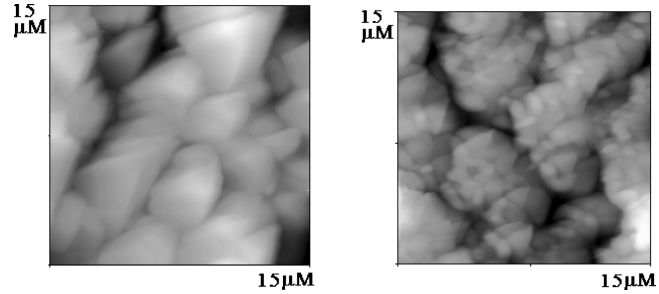

Figure 8. AFM images of pure inulin and the inulin−OTAB complex: (A) 0.5% (w/v) pure inulin; (B) with [OTAB] > C_T.

SEM. The field emission scanning electron microscopic (FESEM) images of inulin without and with OTAB are depicted in Figure 7. Approximately spherical to somewhat elongated entities of pure inulin were observed to form (Figure 7A); their sizes were much bigger than that observed in the TEM picture (Figure 6A). The sizes of the inulin species grew while drying on the smooth solid surface and while sampling, which produced microspheres with internal cracks and an average diameter of 4 μm (inset Figure 7A). Interconnected microspheres were also found. By interaction with OTAB at C_T, the surface morphology of the microspheres changed; the coacervates were densely assembled (Figure 7B). The overall texture was network-like.

AFM. The AFM phase contrast images of pure inulin and its complex with OTAB at C_T are illustrated in panels A and B of Figure 8, respectively. A clear morphological change in inulin was observed by interaction with OTAB. There were striking dissimilarities in their topologies. Pure inulin appeared as discrete bodies with a smooth surface. The OTAB-complexed coacervates appeared as compact assemblies studded with prolate-type globules. The AFM images were more enlarged compared with the SEM images.

F. Thermal Stability. The thermal stability of the inulin−OTAB complex was studied by TGA, DTA, and DSC techniques. The findings are presented below.

TGA−DTA. The TGA and DTA curves for OTAB-complexed inulin are presented in Figure 9. A sharp weight loss started at 160 °C and continued up to 275 °C. This part was the decomposition range of the complex in the TGA profile. The compound was not found to show a melting temperature; instead, it started to decompose at 160 °C. Pure inulin was

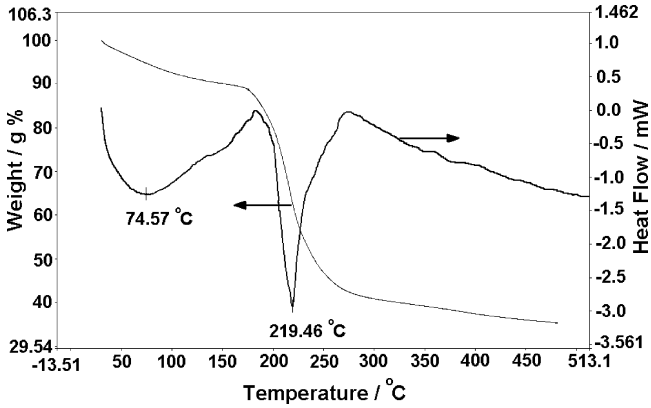

Figure 9. TGA and DTA profiles for the isolated inulin−OTAB complex (22.7 g/g).

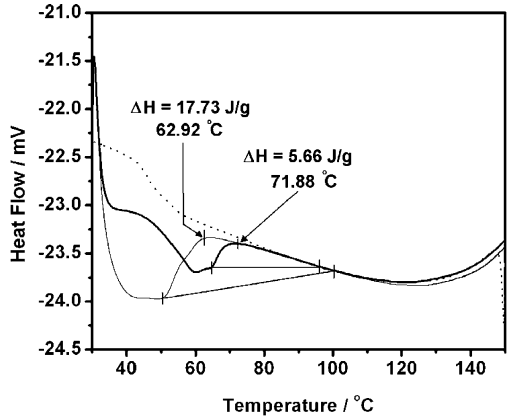

Figure 10. DSC profiles for the isolated inulin−OTAB complex (22.7 g/g): heating, —; cooling, •••; reheating, —.

found[55] to produce sharp melting at 165 °C. The disintegration process became mild in the post-275 °C region. DTA produced a broad endothermic region around 75 °C well below the decomposition temperature. A structural change in the soft complex molecule was envisaged. This was followed by a large and sharp endothermic decomposition process around 220 °C.

DSC. DSC profiles for heating, cooling, and reheating of the OTAB-complexed inulin in the temperature range of 30−150 °C (lower than its decomposition range) are depicted in Figure 10. The first heating produced an endothermic transition with $\Delta H = 5.66$ J g^{-1} around 72 °C. The cooling curve showed hysterisis at temperatures <72 °C. The second heating curve produced a higher endothermic enthalpy change of 17.73 J g^{-1} at 63 °C. The endothermic transition in reheating was associated with a larger heat change with a shift toward lower temperature. The three representations depicted sizable differences in the region below 72 °C.

Conclusions

The cationic surfactants, C_nTAB, bind with inulin which strengthens with an increase in alkyl chain length. Amphiphile hydrophobicity has a distinct impact on the process. The studied C_nTAB representatives C_{12}-, C_{14}-, C_{16}- and C_{18}TAB are found to form cac and the extended cmc$_e$ at C_f. The cac decreases with increasing chain length but cmc$_e$ for C_{12}- and C_{14}TAB are only marginally different from the normal cmc. In general, tensiometry produces cac, C_S (the point of maximum turbidity representing associated coacervate formation), and C_f for all the C_nTAB homologues which are not evidenced by the other methods. The appearances of C^*, C_S, and C_f are formed for C_{18}TAB by conductometry, turbidimetry, and viscometry which are absent for lower homologues than C_{18}. The C_{18}TAB, thus, evidence distinct differences in its behavior in an inulin solution from the rest of the homologues. The $\Gamma^{C_f}_{max}$ and $A^{C_f}_{min}$ increases and decreases, respectively, with an increase in the chain length of the amphiphiles. There is a reverse in their orders with an increase in inulin concentration in the system. The $\Delta G^0_{ad} > \Delta G^0_{C_f}$; the average values of their ratios is 1.35 (the former is 35% more spontaneous than the latter). The parameter $(C_f - \text{cac})/\text{cac}$ increases with C_n; they follow a fairly linear course. The cmc$_e$ has a direct correlation with the amphiphile chain length. Pure inulin molecules aggregate in aqueous solution producing fairly homogeneous globule-like species. In the presence of [OTAB] < C_T, the morphology of the polymer assemblies changes; it becomes heterogeneous with varied shapes. At [OTAB] > C_T, the large aggregates disintegrate into smaller sizes. Their SEM and AFM measurements evidence smooth appearances. The OTAB-complexed product appears as condensed loop-like networks in SEM and appears like agglomerated beads in AFM. Similar features of inulin interaction with other C_nTABs are expected. While pure inulin sharply melts at 165 °C, its OTAB complex melts with decomposition between 160 and 275 °C. A broad endothermic structural transition around 75 °C followed by a sharp endothermic decomposition around 220 °C has been observed for the OTAB-complexed inulin from DTA measurements. The DSC results produce fair hysteresis at temperatures <72 °C with exothermic structural transitions both for the first and for the second heating runs. The reheating transition is associated with increased enthalpy in the lower temperature range than in the first heating. One cycle of heating and cooling increases the thermal instability of the complex.

Acknowledgment. A.D. thanks UGC, government of India, for a senior research fellowship. Financial support from the Indian National Science Academy to S.P.M. is thankfully acknowledged. Financial support from the Center for Advanced Studies, Department of Chemistry, Jadavpur University is acknowledged. We thank Dr. A. J. Pal and Dr. A. Bhaumik of the Department of Solid State Physics and Centre for Advanced Materials, and the Department of Materials Science and Centre for Advanced Materials, IACS, respectively, for using their AFM and TEM facilities. The cooperation of Dr. K. Dhara, Mr. K. Sarkar, and Mr. B. C. Das, for SEM, TEM, and AFM measurements, respectively, is appreciated.

References and Notes

(1) Chavanpatil, M. D.; Khdair, A.; Patil, Y.; Handa, H.; Mao, G.; Panyam, J. *J. Pharm. Sci.* **2007**, *96*, 3379.
(2) Kapoor, Y.; Chauhan, A. *J. Colloid Interface Sci.* **2008**, *322*, 624.
(3) Griffiths, P. C.; Khayat, Z.; Tse, S.; Heenan, R. K.; King, S. M.; Duncan, R. *Biomacromolecules* **2007**, *8*, 1004.
(4) Prescott, F. J.; Hahnel, E.; Day, D. *Drug Cosmet. Ind.* **1963**, *93*, 443 and 540.
(5) Ward, J. B.; Speradio, G. J. *J. Soc. Cosmet. Chem.* **1964**, *15*, 32.
(6) Hannan, R. B.; Goddard, E. D.; Faucher, J. A. *Text. Res. J.* **1978**, *48*, 57.
(7) Shervani, Z.; Ikushima, Y.; Sato, M.; Kawanami, H.; Hakuta, Y.; Yokoyama, T.; Nagase, T.; Kuneida, H.; Aramaki, K. *Colloid Polym. Sci.* **2008**, *286*, 403.
(8) Baimark, Y.; Srisa-ard, M.; Threeprom, J.; Narkkong, N.-A. *Colloid Polym. Sci.* **2007**, *285*, 1521.
(9) Carswell, A. D. W.; O'Rear, E. A.; Grady, B. P. *J. Am. Chem. Soc.* **2003**, *125*, 14793.
(10) Ali, D.; Bolton, S.; Gaylord, G. *J. Appl. Polym. Sci.* **1991**, *42*, 947.
(11) Kilau, H. W.; Voltz, J. I. *Colloids Surf.* **1991**, *57*, 17.
(12) Somasundaran, P.; Lee, L. T. *Sep. Sci. Technol.* **1981**, *16*, 1475.
(13) Somasundaran, P.; Cleverdon, J. *Colloids Surf.* **1985**, *13*, 73.

(14) Francois, J.; Dayantis, J.; Sabbadin, J. *Eur. Polym. J.* **1985**, *43*, 491.
(15) Zana, R.; Lianos, P.; Lang, J. *J. Phys. Chem.* **1985**, *89*, 41.
(16) Maltesh, C.; Somasundaran, P. *Langmuir* **1992**, *8*, 1926.
(17) Brown, W.; Fundin, J.; de Graca Miguel, M. *Macromolecules* **1992**, *25*, 7193.
(18) Dai, S.; Tam, K. C. *J. Phys. Chem. B* **2001**, *105*, 10759.
(19) Xia, Y.-M.; Fang, Y.; Liu, X.-F.; Cai, K. *Colloid Polym. Sci.* **2002**, *280*, 479.
(20) Prasad, M.; Palepu, R.; Moulik, S. P. *Colloid Polym. Sci.* **2006**, *284*, 1453.
(21) Wang, G.; Olofsson, G. *J. Phys. Chem. B* **1998**, *102*, 9276.
(22) Roscigno, P.; Asaro, F.; Pellizer, G.; Ortona, O.; Paduano, L. *Langmuir* **2003**, *19*, 9638.
(23) Mangiapia, G.; Berti, D.; Baglioni, P.; Teixeira, J.; Paduano, L. *J. Phys. Chem. B* **2004**, *108*, 9772.
(24) Sesta, B.; D'Aprano, A.; Segre, A. L.; Proietti, N. *Langmuir* **1997**, *13*, 6612.
(25) Li, F.; Li, G.-Z.; Xu, G.-Y.; Wang, H.-Q.; Wang, M. *Colloid Polym. Sci.* **1998**, *276*, 1.
(26) Dan, A.; Chakraborty, I.; Ghosh, S.; Moulik, S. P. *Langmuir* **2007**, *23*, 7531.
(27) Trabelsi, S.; Langevin, D. *Langmuir* **2007**, *23*, 1248.
(28) Biswas, S. C.; Chattoraj, D. K. *Langmuir* **1997**, *13*, 4512.
(29) Chakraborty, T.; Chakraborty, I.; Ghosh, S. *Langmuir* **2006**, *22*, 9905.
(30) Hait, S. K.; Majhi, P. R.; Blume, A.; Moulik, S. P. *J. Phys. Chem. B* **2003**, *107*, 3650.
(31) Burke, S. E.; Palepu, R. M.; Hait, S. K.; Moulik, S. P. *Colloid Polym. Sci.* **2003**, *122*, 47.
(32) Merta, J.; Tammelin, T.; Stenius, P. *Colloids Surf., A* **2004**, *250*, 103.
(33) Merta, J.; Stenius, P. *Colloid Polym. Sci.* **1995**, *273*, 974.
(34) Lundqvist, H.; Eliasson, A.-C.; Olofsson, G. *Carbohydr. Polym.* **2002**, *49*, 43.
(35) Yamamoto, M.; Sano, T.; Harada, S.; Yasunaga, T. *Bull. Chem. Soc. Jpn.* **1983**, *56*, 2643.
(36) Hui, Y.; Russell, J. C.; Whitten, D. G. *J. Am. Chem. Soc.* **1983**, *105*, 1374.
(37) Moulik, S. P.; Gupta, S. *Carbohydr. Res.* **1979**, *71*, 251.
(38) de Miranda, J. A.; Cacita, N.; Okano, L. T. *Colloids Surf., B* **2007**, *60*, 19.
(39) Fishman, M. M.; Freund, I. *J. Colloid Sci.* **1961**, *16*, 392.
(40) Lundqvist, H.; Nilsson, G. S.; Eliasson, A.-C.; Gorton, L. *Starch/Staerke* **2002**, *54*, 100.
(41) Mehta, S. K.; Bhawna; Bhasin, K. K.; Kumar, A. *J. Colloid Interface Sci.* **2008**, *323*, 426.
(42) Singh, R. B.; Mahanta, S.; Guchhait, N. *Chem. Phys. Lett.* **2008**, *463*, 183.
(43) Singh, M. *J. Appl. Polym. Sci.* **2008**, *110*, 2293.
(44) Maulik, S.; Dutta, P.; Chattoraj, D. K.; Moulik, S. P. *Colloids Surf., B* **1998**, *11*, 1.
(45) Chatterjee, A.; Moulik, S. P.; Majhi, P. R.; Sanyal, S. K. *Biophys. Chem.* **2002**, *98*, 313.
(46) Mitra, D.; Bhattacharya, S. C.; Moulik, S. P. *J. Phys. Chem. B* **2008**, *112*, 6609.
(47) Moreira, L. M.; Santiago, P. S.; de Almeida, E. V.; Tabak, M. *Colloids Surf., B* **2008**, *61*, 153.
(48) Chakraborty, T.; Chakraborty, I.; Moulik, S. P.; Ghosh, S. *J. Phys. Chem. B* **2007**, *111*, 2736.
(49) Ghosh, S. *Colloids Surf., A* **2005**, *264*, 6.
(50) Ghosh, S. *Colloids Surf., B* **2005**, *41*, 209.
(51) Mehta, S. K.; Bhawna; Kaur, K.; Bhasin, K. K. *Colloids Surf., A* **2008**, *317*, 32.
(52) Khanal, A.; Li, Y.; Takisawa, N.; Kawasaki, N.; Oishi, Y.; Nakashima, K. *Langmuir* **2004**, *20*, 4809.
(53) Bronich, T. K.; Cherry, T.; Vinogradov, S. V.; Eisenberg, A.; Kabanov, V. A.; Kabanov, A. V. *Langmuir* **1998**, *14*, 6101.
(54) Yao, J.-H.; Mya, K. Y.; Li, X.; Parameswaran, M.; Xu, Q.-H.; Loh, K. P.; Chen, Z.-K. *J. Phys. Chem. B* **2008**, *112*, 749.
(55) Dan, A.; Ghosh, S.; Moulik, S. P. *Biopolymers* (published, DOI: 10.1002/bip.21199).
(56) De Bruyn, A.; Alvarez, A. P.; Sandra, P.; De Leenheer, L. *Carbohydr. Res.* **1992**, *235*, 303.
(57) Van Loo, J.; Cummings, J.; Delzenne, A.; Englyst, H.; Franck, A.; Hopkins, M.; Kok, N.; Macfarlane, G.; Newton, D.; Quigley, M.; Roberfroid, M.; van den Heuvel, E. *Br. J. Nutr.* **1999**, *81*, 121.
(58) Stevens, C. V.; Meriggi, A.; Booten, K. *Biomacromolecules* **2001**, *2*, 1.
(59) Moulik, S. P.; Haque, M. E.; Jana, P. J.; Das, A. R. *J. Phys. Chem.* **1996**, *100*, 701.
(60) Basu Ray, G.; Chakraborty, I.; Ghosh, S.; Moulik, S. P.; Palepu, R. *Langmuir* **2005**, *21*, 10958.
(61) Maiti, K.; Chakraborty, I.; Bhattacharya, S. C.; Panda, A. K.; Moulik, S. P. *J. Phys. Chem. B* **2007**, *111*, 14175.
(62) Evans, H. C. *J. Chem. Soc.* **1956**, 579.
(63) Miller, D. D.; Lenhart, W.; Antalek, B. J.; Williams, A. J.; Hewitt, J. M. *Langmuir* **1994**, *10*, 68.
(64) Taylor, D. J. F.; Thomas, R. K.; Hines, J. D.; Humphreys, K.; Penfold, J. *Langmuir* **2002**, *18*, 9783.
(65) Whitesides, T. H.; Miller, D. D. *Langmuir* **1994**, *10*, 2899.
(66) Goddard, E. D. *Colloids Surf.* **1986**, *19*, 255.
(67) Goddard, E. D. *J. Colloid Interface Sci.* **2002**, *256*, 228.
(68) Guillot, S.; Delsanti, M.; Desert, S.; Langevin, D. *Langmuir* **2003**, *19*, 230.
(69) Ghosh, B. N.; Bandopadhya, S.; Moulik, S. P. *Proc. Natl. Inst. Sci. India* **1961**, *27*, 193.
(70) Ghosh, B. N.; Moulik, S. P.; Sen Gupta, S. K. *J. Electroanal. Chem.* **1965**, *9*, 372.
(71) Mandal, A. B.; Ray, S.; Biswas, A. M.; Moulik, S. P. *J. Phys. Chem.* **1980**, *84*, 856.
(72) Moulik, S. P. *Electrochim. Acta* **1973**, *18*, 981.
(73) Asnacios, A.; Langevin, D.; Argillier, J. F. *Eur. Phys. J. B* **1998**, *5*, 905.
(74) Lundin, M.; Macakova, L.; Dedinaite, A.; Claesson, P. *Langmuir* **2008**, *24*, 3814.
(75) Bu, H.; Kjøniksen, A.-L.; Elgsaeter, A.; Nyström, B. *Colloids Surf., A* **2006**, *278*, 166.
(76) Hansson, P.; Almgren, M. *J. Phys. Chem.* **1996**, *100*, 9038.
(77) Nagarajan, R.; Kalpakci, B. *Polym. Prepr. (Am. Chem. Soc., Div. Polym. Chem.)* **1982**, *23*, 41.
(78) Turro, N. J.; Lie, X.-G.; Ananthapadmanabhan, K. P.; Aronson, M. *Langmuir* **1995**, *11*, 2525.
(79) Cabane, B.; Duplessix, R. *J. Phys. (Paris)* **1982**, *43*, 1529.
(80) Wang, C.; Palaniswamy, R.; Tam, K. C. *Langmuir* **2006**, *22*, 2927.
(81) Castro, E.; Taboada, P.; Barbosa, S.; Mosquera, V. *Biomacromolecules* **2005**, *6*, 1438.

JP902641D